

Fabrication of high-quality PMMA/SiO_x spaced planar microcavities for strong coupling of light with monolayer WS₂ excitons

Tinghe Yun,^{1,2,3} Eliezer Estrecho,¹ Andrew G. Truscott,⁴ Elena A. Ostrovskaya,^{1,*} and Matthias J. Wurdack^{1,†}

¹*ARC Centre of Excellence in Future Low-Energy Electronics Technologies and Department of Quantum Science and Technology, Research School of Physics, The Australian National University, Canberra, ACT 2601, Australia*

²*Songshan Lake Materials Laboratory, Dongguan 523808, Guangdong, China*

³*Institute of Physics, Chinese Academy of Science, Beijing, 100190, China*

⁴*Department of Quantum Science and Technology, Research School of Physics, The Australian National University, Canberra, ACT 2601, Australia*

(Dated: September 29, 2022)

Exciton polaritons in atomically-thin transition metal dichalcogenide crystals (monolayer TMDCs) have emerged as a promising candidate to enable topological transport, ultra-efficient laser technologies, and collective quantum phenomena such as polariton condensation and superfluidity at room temperature. However, integrating monolayer TMDCs into high-quality planar microcavities to achieve the required strong coupling between the cavity photons and the TMDC excitons (bound electron-hole pairs) has proven challenging. Previous approaches to integration had to compromise between various adverse effects on the strength of light-matter interactions in the monolayer, the cavity photon lifetime, and the lateral size of the microcavity. Here, we demonstrate a scalable approach to fabricating high-quality planar microcavities with an integrated monolayer WS₂ layer-by-layer by using polymethyl methacrylate/silicon oxide (PMMA/SiO_x) as a cavity spacer. Because the exciton oscillator strength is well protected against the required processing steps by the PMMA layer, the microcavities investigated in this work, which have quality factors of above 10³, can operate in the strong light-matter coupling regime at room temperature. This is an important step towards fabricating wafer-scale and patterned microcavities for engineering the exciton-polariton potential landscape, which is essential for enabling many proposed technologies.

Planar microcavities with embedded exciton-hosting materials based on the design of vertical-cavity surface-emitting lasers (VCSELs) have enabled the regime of strong light-matter coupling between excitons and photons [1]. The formation of exciton polaritons (polaritons herein), part-light part-matter bosonic quasiparticles, in these semiconductor microcavities has triggered significant research efforts, which led to the creation of Bose-Einstein condensates (BEC) [2] and superfluids [3], the demonstration of non-Hermitian effects [4], the development of electrically-driven ultra-efficient lasers [5] and the realisation of topological edge transport [6] on microchips. By using semiconductors with large exciton binding energies, some of these observations were successfully realised at room temperature [7–14].

A promising family of inorganic semiconductors for future polaritonic devices are atomically-thin TMDCs [15–19]. However, integrating these monolayers into planar microcavities to create polaritons has turned out to be challenging because they are extremely fragile and easily damaged by various fabrication techniques [20]. Many attempts at TMDC integration by using metallic top mirrors [19, 21] or depositing the top structures directly on top of the monolayer with aggressive material deposition techniques [16, 22], have led to dramatic degradation of the photon lifetimes, exciton quantum yields, or exciton-photon coupling strengths. These properties are significantly improved by recent techniques for integrating TMDCs into all-dielectric microcavities. How-

ever, these approaches are based on micrometer-sized distributed Bragg reflector (DBR) chips [23–27] or mechanically exfoliated hexagonal Boron Nitride (hBN) crystals [28, 29], which massively limit its technological scalability. While all of these approaches have enabled the demonstration of many striking effects of TMDC polaritons [16, 18], which include signatures of bosonic condensation [26, 30], the spin-valley Hall effect [23], and ballistic propagation at room temperature [25], fabrication recipes which allow for both scalability and high performance of the final device to enable future TMDC polariton based technologies are still to be developed.

In this work, we introduce a method for integrating monolayer WS₂ into high-quality planar microcavities with the lateral size mainly limited by the size of the monolayer. In particular, we layer PMMA/SiO_x on top of the monolayer before depositing the top DBR via plasma enhanced chemical vapour deposition (PECVD). This is in contrast to using metal as the top mirror of the cavity as was done for the heavily investigated DBR/metal cavities [19, 21, 31–34]. We study the effects of each processing step on the optical properties of the WS₂ monolayer showing that the exciton oscillator strength is well preserved inside these structures, which enables strong light-matter coupling at room temperature. Finally, we demonstrate that the quality factors (Q-factors) of these microcavities can reach values on the order of 10³, therefore exceeding the Q-factors of DBR/metal cavities by 1 – 2 orders of magnitude

[21, 31, 32, 34] (see Supplementary Table S1). TMDC based microcavities with comparable Q-factors were previously only realised on microchips by using the technologies that inherently limit the lateral size of the devices [23–25, 28] or dramatically strain the monolayer [29, 35].

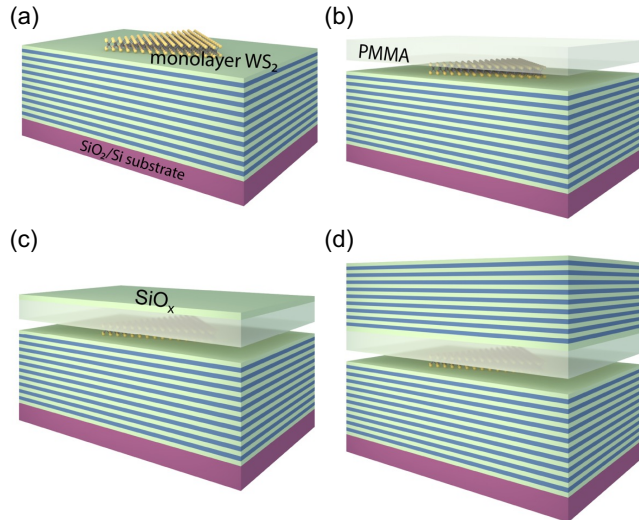


FIG. 1. **Design and fabrication procedure for the microcavity.** (a-d) Schematics of the fabrication steps starting from (a) assembly of the base structure consisting of a $\text{TiO}_2/\text{SiO}_2$ DBR substrate and a monolayer WS_2 , followed by (b) the deposition of the PMMA and (c) SiO_x layers, and finished by (d) the deposition of the top $\text{SiN}_x/\text{SiO}_x$ DBR via PECVD.

The fabrication procedure for the PMMA/ SiO_x spaced planar microcavities tested and discussed in this work is schematically demonstrated in Fig. 1a-d. The $\text{TiO}_2/\text{SiO}_2$ DBR substrate, which consists of 17.5 mirror pairs, is fabricated via sputtering [36] and finishes with a SiO_2 capping layer that has a thickness corresponding to half of the cavity spacer. After transferring the monolayer onto the substrate (see Fig. 1a), a PMMA layer is spin-coated on top, which acts both as a protection layer and a cavity spacer (see Fig. 1b). The remaining part of the cavity-spacer (SiO_x) and the top DBR ($\text{SiN}_x/\text{SiO}_x$), starting with the SiN_x layer, are deposited via PECVD at 150 °C to finalise the microcavity (see Fig. 1c-d and Supplementary Section S2 for details). The SiO_x spacer allows us to fine-tune the cavity energy and also prevents cracking of the top DBR, which we found to occur when directly depositing it onto PMMA. Most effective confinement of photons with the wavelength λ_C is achieved when the total cavity spacer and each DBR layer have a thickness of $\lambda_C/2n$ and $\lambda_C/4n$, respectively, where n is the respective refractive index of each layer [37]. In principle, the DBR substrate can be fabricated with any deposition technique suitable for making highly reflective DBRs with a smooth, high-quality layer finish.

To understand the effect of PMMA deposition on the

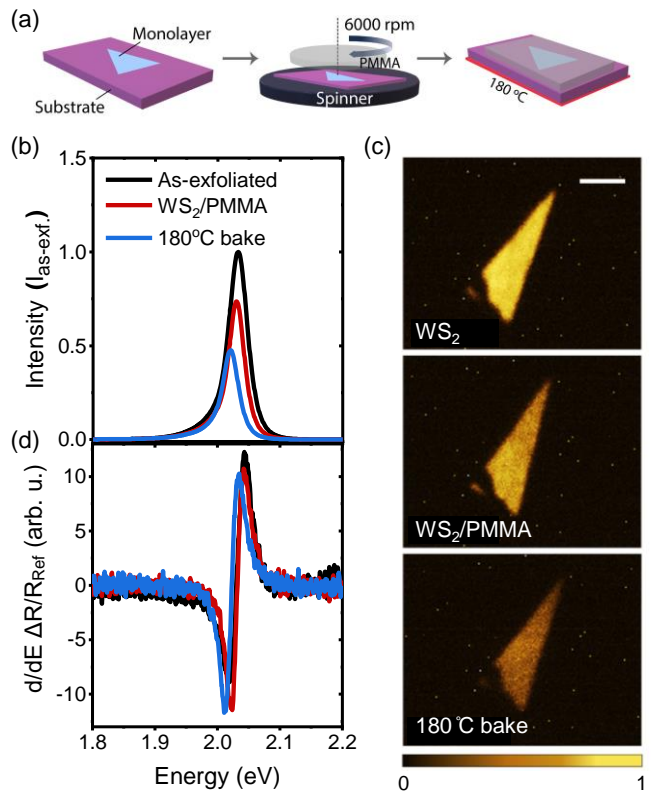


FIG. 2. **Effects of PMMA on the optical properties of WS_2 .** (a) Schematics of the PMMA encapsulation process. (b-c) Comparison of (b) the PL spectra, (c) the corresponding PL maps, and (d) the derivative of the reflectance contrast spectra for the as-exfoliated monolayer, monolayer capped by PMMA, and the PMMA-capped monolayer baked at 180 °C. The scale bar size in panel (c) is 10 μm .

optical properties of monolayer WS_2 (see Fig. 1b), we mechanically exfoliated a monolayer (bulk crystals sourced from HQ Graphene [38]) on commercial SiO_2/Si substrates (sourced from Nova materials [39]). A 80 nm layer PMMA (molecular weight $\sim 950,000$ g/mol dissolved in anhydrous anisole with a 2.2% concentration) was then spin-coated on top of the monolayer at 6000 rpm for 60 s (see Fig. 2a). To fully remove the anisole residues and ensure a high-quality surface finish, the PMMA was hard baked at 180 °C for 90 s [21].

The tests of the optical response of the WS_2 excitons were performed via real-space photoluminescence (PL) and white-light reflectivity measurements under ambient conditions. For the PL studies, we excited the samples with a large Gaussian spot ($d \approx 25 \mu\text{m}$) from a frequency doubled ND:YAG continuous wave (cw) 532-nm laser source with the excitation energy ($E \approx 2.33$ eV [40]) above the A-valley exciton energy of monolayer WS_2 [41]. The reflectivity spectra were measured under illumination of the sample surface with a tungsten halogen white light source. The PL spectra were obtained by averaging the signal from a small sample area, and the derivative

of the reflectance contrast spectra $d(\Delta R/R_{\text{ref}})/dE$ was derived by also measuring the white light reflection next to the monolayer as reference R_{ref} , with $\Delta R = R - R_{\text{ref}}$. Since the product of linewidth and amplitude of the reflectance contrast spectrum at the excitonic resonance scales with the exciton oscillator strength, it quantifies the light-matter interaction in the monolayer [18, 42] required for the strong exciton-photon coupling regime.

The PL spectra in Fig. 2b show the PL quenching after the capping of monolayer WS_2 with PMMA, and further degradation after baking it. This change is also seen in the corresponding PL maps (see Fig. 2c). The pronounced PL quenching effect is possibly due to the chemical instability of this material. WS_2 crystals are normally n-type semiconductors due to the presence of sulphur vacancies [43–46], and therefore, they can be strongly affected by the surrounding molecules [47], such as organic and water molecules that can act as dopants [48]. As a consequence, the PMMA capping process can modify the doping level of the monolayer effectively causing a reduction of the exciton quantum yield [47]. The additional decrease of the exciton PL after the baking process is likely caused by the elevated temperature accelerating the aging process (oxidation) of the monolayer, which further decreases the exciton quantum yield [49]. However, the derivative of the reflectance contrast spectra in Fig. 2d reveals that the exciton oscillator strength is barely affected after the PMMA capping and baking, which indicates that PMMA encapsulation will have a negligible effect on the exciton-photon interactions.

Since the monolayers are fragile and easily damaged by many fabrication techniques including PECVD [20], we further tested how well the PMMA layer protects the monolayer against PECVD of SiO_x . The influence of the deposition on the exciton PL and absorption in the PMMA-capped monolayer WS_2 is demonstrated in Fig. 3a-b. Clearly, the exciton PL intensity significantly decreases after the deposition process. The observed quenching is stronger with a larger SiO_x thickness, which scales with the duration of the deposition. Between the layer thicknesses of $1.2 \mu\text{m}$ SiO_x and $1.8 \mu\text{m}$ SiO_x the PL intensity remains constant and yields $\sim 25\%$ of the PL intensity of the PMMA-capped WS_2 , which shows that PECVD induced PL quenching saturates at this level. Similarly, the exciton absorption shown in Fig. 3b also decreases after material deposition. This degradation of the PL and oscillator strength could be attributed to the penetration of gaseous plasma (leakage of conductive ions) through the microporous PMMA layer [50]. Once the plasma reaches the monolayer surface, it can degrade the material by creating additional defects, which explains the observed behaviour. Nevertheless, the decrease of excitonic absorption after material deposition is much less compared to that of the excitonic PL. Accordingly, the oscillator strength remains relatively high after deposition of PMMA and SiO_x in contrast with the exciton

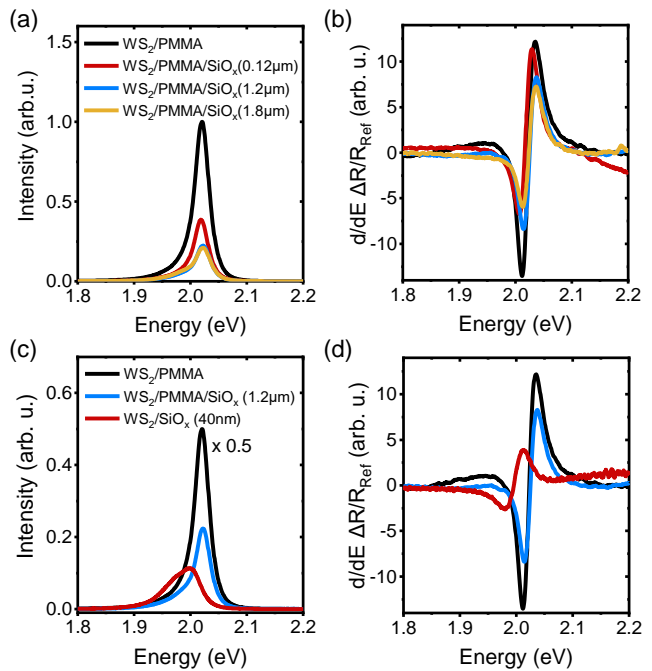


FIG. 3. **Effects of PECVD deposition on the optical properties of WS_2 with and without PMMA passivation.** (a-b) Comparison of (a) the PL and (b) the derivative of the reflectance contrast spectra for monolayer WS_2 capped with PMMA, and further overgrown with SiO_x of different thicknesses by PECVD. (c-d) Comparison of (c) the PL spectra and (d) the derivative of the reflectance contrast spectra of monolayer WS_2 after deposition of (black) PMMA, (blue) PMMA/ SiO_x and (red) SiO_x .

quantum yield.

To further test the protective properties of the PMMA layer, we prepared an uncapped monolayer sample, on which we directly deposited 40 nm of SiO_x via PECVD. This thickness was chosen to maintain some optical response from the exciton in the WS_2/SiO_x structure [20]. The PL spectra in Fig. 3c reveal that the PL emission of PMMA-capped monolayers with subsequent $1.2 \mu\text{m}$ SiO_x deposition is almost twice as strong as that of the uncapped monolayer after deposition of 40 nm SiO_x . The reflectance contrast spectra (see Fig. 3d) also show much stronger degradation of the exciton oscillator strength for the uncapped monolayer compared to the capped one. Furthermore, the uncapped monolayer shows a pronounced shoulder in the PL spectrum at $E \approx 1.97 \text{ eV}$ likely stemming from trion emission [44, 51, 52], which indicates a significant defect-induced charge doping effect caused by the deposition process [20, 46, 53]. These results clearly highlight that the PMMA layer protects the monolayer against the dielectric deposition by PECVD. Since the thickness of deposited SiO_x is directly related to the duration of exposure to plasma, the PMMA-capped monolayer was exposed to the plasma for 30 times longer, but still maintained a larger excitonic response, which

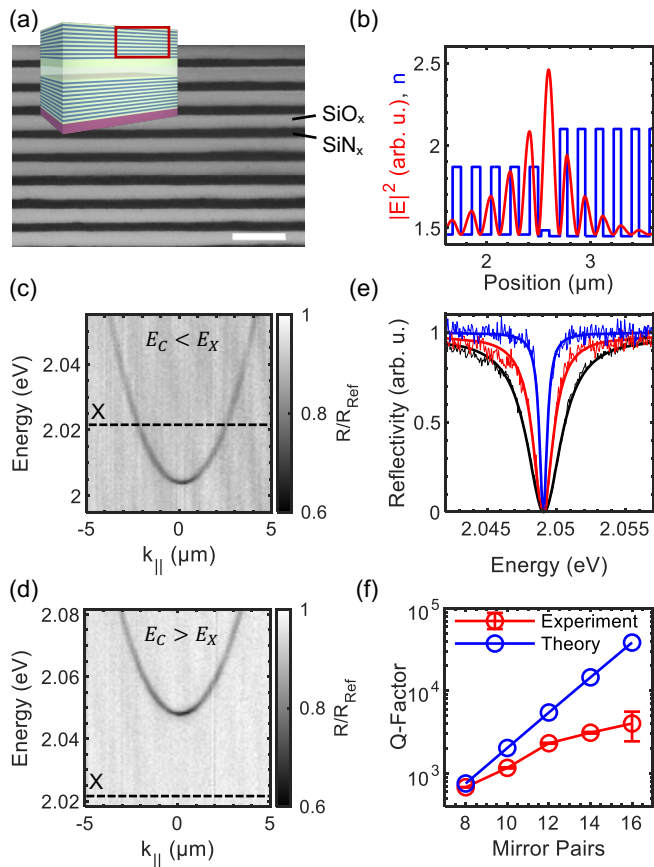


FIG. 4. **Design and characterisation of an empty microcavity.** (a) The SEM image of a $\text{SiO}_x/\text{SiN}_x$ DBR fabricated by PECVD on top of PMMA as marked in (inset) the schematics of the empty microcavity. The scale bar size is 500 nm. (b) The (blue) refractive indices of the layers around the centre of the microcavity and (red) the simulated E-field distribution of the cavity mode. (c,d) Angle-resolved reflectivity spectra of microcavities with the resonance energies (c) negatively and (d) positively detuned from the (X) WS_2 exciton energy at room temperature. (e) Reflectivity spectra at normal incidence with (black) 8.5, (red) 10.5 and (blue) 14.5 $\text{SiN}_x/\text{SiO}_x$ top DBR mirror pairs. (f) Q-factor of the microcavity as a function of top DBR mirror pairs.

confirms the protective function of the PMMA layer.

In addition to testing how PMMA and dielectric material deposition affect the optical response of the WS_2 excitons at room temperature, we determined the quality of the photon mode that can be achieved in our cavity without the integration of a monolayer. To ensure that the PMMA/ SiO_x cavity provides a suitable substrate for the top DBR, we perform scanning electron microscope (SEM) imaging on the cross-section of a $\text{SiN}_x/\text{SiO}_x$ DBR grown on top of a PMMA layer via PECVD (see Fig. 4a). The SEM image reveals that the SiO_x and SiN_x layers have a consistent thickness throughout the mirror and a smooth lateral profile on the scale of the light wavelength that is crucial for high optical performance.

Figure 4b presents the simulation of the optical E-field distribution inside an empty cavity with a cavity-length of $\lambda_C/2n$ fulfilling the Bragg condition for $\lambda_C = 615$ nm, performed with the transfer matrix method [54]. As usual for $\lambda/2$ -cavities [37], the strongly confined resonant E-field has its maximum near the centre of the cavity, which allows for maximum energy exchange between photons and excitons when the monolayer is placed at this position. This is ensured by our sample design, where the last layer of the DBR substrate corresponds to the first half of the cavity spacer. By varying the thickness of the SiO_x layer on top of the PMMA layer, both having a similar refractive index, we can fine-tune the cavity length d , and therefore, the cavity mode energy E_C . This, in turn, enables control of the exciton-photon detuning: $\Delta = E_C - E_X$, where E_X is the exciton energy.

The angle-resolved reflectivity spectra for empty cavities with 110 nm and 95 nm of PMMA/ SiO_x spacer are presented in Fig. 4c-d, respectively, with the top DBRs consisting of 13.5 $\text{SiN}_x/\text{SiO}_x$ mirror pairs. The spectra clearly demonstrate the characteristic parabolic dispersion of the cavity photons and show that the photon energy can be tuned well across the exciton energy. The linewidth of the cavity photon FWHM_C can be controlled with the number of mirror pairs of the top DBR (see Fig. 4e), which allows us to increase the quality factor $Q = E_C/\text{FWHM}_C$ to $Q \approx 4 \cdot 10^3$ reaching the resolution limit of our optical setup (see Fig. 4f). These results demonstrate that this sample design enables a good control over both the cavity photon energy and linewidth and allows us to reach much higher Q-factors compared to those of the similarly constructed DBR/metal cavities, e.g., [19, 21, 32] (see Supplementary Table S1). However, to change the exciton-photon detuning, the sample needs to be reproduced with a different thickness of the cavity spacer, and the achievable Q-factors are smaller than the theoretically expected values (see Fig. 4f). The growth of the Q-factor with the number of mirror pairs in the top DBR decreases above 12 pairs, likely due to scattering and absorption processes in the dielectric layers.

Finally, we fabricated the whole microcavity with an integrated monolayer WS_2 , as schematically shown in Fig. 1. Figure 5a presents the PL spectrum of a monolayer WS_2 placed on the DBR substrate, after deposition of the PMMA spacer (see Fig. 1b). When fitting the spectrum with a three peak Voigt-function accounting for the localised, charged and neutral exciton emission [44] (see Fig. 5a), we can extract the energy and the linewidth of the neutral exciton peak: $E_X \approx 2.013$ eV and $\text{FWHM}_X \approx 35$ meV, with a contribution of homogeneous broadening $\text{FWHM}_X^H \approx 12$ meV and inhomogeneous broadening $\text{FWHM}_X^{IH} \approx 28$ meV. The large spectral weight of the neutral exciton is an evidence of the high quality of the DBR substrate causing negligible doping [53] or strain effects [56, 57] in the monolayer,

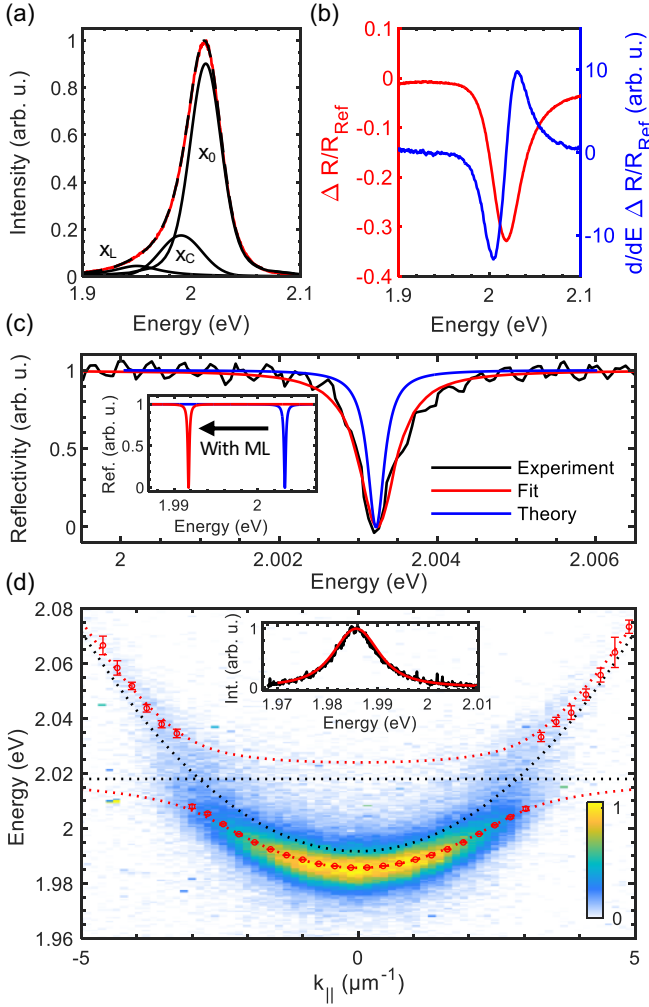


FIG. 5. **Characterisation of the microcavity with an integrated monolayer WS₂.** (a) PL spectrum of a monolayer WS₂ on top of the DBR substrate fitted with (black) a three peak Voigt function accounting for (X_L) localised, (X_C) charged and (X₀) neutral excitons. (b) Reflectance contrast spectrum of the monolayer WS₂ and its derivative. (c) Reflectivity spectrum of the cavity around the photon energy at normal incidence next to the position of the monolayer fitted with a (red) Lorentzian function; (blue) theoretical reflectivity spectrum calculated via transfer matrix calculations. (inset) Calculated photon energies at $k_{\parallel} = 0$ with and without the monolayer (ML). The cavity energy is shifted by ~ 11.4 meV due to the optical thickness of the monolayer ($d_{\text{WS}_2} \approx 0.7$ nm [41], $\epsilon_B^{\text{WS}_2} \approx 15.831$ [55]). (d) Angle-resolved PL spectrum of the full microcavity. The dotted black lines correspond to the experimentally determined exciton and photon energies (see panels a-c), the red dotted lines are the resulting lower and upper polariton branches Eq. (1) with $V = (15.3 \pm 0.3)$ meV and the red circles are the fitted peak energies (see Supplementary Section S3). (Inset) (black) measured and (blue) calculated PL peak of the lower polariton at $k_{\parallel} = 0$.

which can reduce exciton-photon interactions and prevent strong light-matter coupling.

The reflectance contrast spectrum and its derivative with respect to the energy (see Fig. 5b) reveal the exciton energy $E_X \approx 2.018$ eV and linewidth $\text{FWHM}_X \approx 35$ meV, which is in agreement with the Stokes shifted exciton peak of the PL spectrum, and show a significant exciton oscillator strength in the monolayer that ensures a robust exciton-photon interaction strength.

After deposition of the SiO_x spacer and the top DBR consisting of 13.5 SiN_x/SiO_x layer pairs, we characterise the cavity mode away from the monolayer area. Figure 5c shows the measured and theoretical reflectivity spectra of the microcavity with the cavity mode energy $E_C(k_{\parallel} = 0) \approx 2.0032$ eV and linewidths $\text{FWHM}_C^{\text{Exp}} = (565 \pm 13)$ μeV and $\text{FWHM}_C^{\text{Th}} = 257$ μeV , respectively. While the corresponding measured Q-factor $Q^{\text{Exp}} \approx 3500$ is smaller than the theoretical Q-factor $Q^{\text{Th}} \approx 7800$, it is similar to the Q-factor of the empty microcavity (see Fig. 4f) and in general, comparable to the largest values reached for microcavities with embedded TMDCs [24, 25, 28, 29, 58] (see Supplementary Table S1).

Figure 5d presents the angle-resolved PL measurement of the whole structure, which was obtained via excitation of the monolayer with a tightly focused laser spot ($\lambda = 532$ nm) and collecting the PL in momentum space with a NA=0.65 objective, projected into a 2D spectrometer. The measured dispersion, which decreases in intensity at larger energies due to thermalisation [21, 25], can be approximated with the model of two coupled oscillators [59]:

$$\bar{E}_{U/L} = 0.5 \left(\bar{E}_X + \bar{E}_C \pm \sqrt{(\Delta - i\delta)^2 + 4V^2} \right), \quad (1)$$

where $\bar{E} = E - i\gamma$ are the complex energies of the lossy modes, V is the strength of coupling between the cavity photons and the excitons, and $\delta = \gamma_C - \gamma_X$ (see Fig. 5d). Note, that γ corresponds to HWHM of the measured modes [59].

Using the energies and linewidths of the exciton and cavity resonances (see Fig. 5a-c), we find an excellent agreement between Eq. (1) and the measured dispersion with $V = (15.3 \pm 0.3)$ meV (see Fig. 5d). The corresponding Hopfield coefficient of the lower polariton branch

$$|X|^2 = 0.5 \left[1 + \frac{\Delta}{\sqrt{\Re(\sqrt{4V^2 - \delta^2}) + \Delta^2}} \right] \quad (2)$$

allows us to approximate the polariton PL spectrum with a Voigt profile, where $\text{FWHM}_L^{\text{IH/H}} = |X|^2 \text{FWHM}_X^{\text{IH/H}} + (1 - |X|^2) \text{FWHM}_C^{\text{IH/H}}$, which reproduces the measured PL well (see Fig. 5d, inset). Since $V > |\delta|/2 \approx 8.6$ meV and $V > 0.5\sqrt{\gamma_X^2 + \gamma_C^2} \approx 8.8$ meV, the sample operates in the strong exciton-photon coupling regime, exhibiting

distinct exciton-polariton modes [59]. Hence, the sample fabrication technology presented here is suitable for making high-Q planar microcavities with an integrated atomically-thin WS_2 crystal operating in the strong light-matter coupling regime.

In summary, we have developed a scalable approach for making high-quality planar microcavities with integrated atomically-thin semiconductors suitable for hosting exciton-polaritons at room temperature. This is achieved by depositing the two DBRs, a monolayer WS_2 and a PMMA/ SiO_x spacer layer-by-layer. We demonstrate that the PMMA layer has only a minor effect on the WS_2 exciton oscillator strength and effectively protects the monolayer against further deposition of the top DBR, which allows for strong light-matter interactions in the structure. Since the PMMA/ SiO_x spacer and the top DBR cover the whole microchip homogeneously, the functional area of the loaded microcavity is mainly limited by the size of the monolayer, which can be scaled up to cm-scale with recently developed synthesis [60, 61] and exfoliation [62, 63] techniques. Further, the PMMA can be easily patterned by lithography methods, paving the way towards creating polariton lattices, waveguides and other 2D potential landscapes on a microchip, as previously demonstrated for microcavities with embedded perovskites [14, 64].

ACKNOWLEDGEMENTS

This work was supported by the Australian Research Council (ARC) grants CE170100039 and DE220100712. We acknowledge the Australian National Fabrication Facility (ANFF) OptoFab at its node in the Australian Capital Territory (ACT) for fabricating the DBR substrate and technical support for sample fabrication from the ANFF ACT node.

* elena.ostrovskaya@anu.edu.au

† matthias.wurdack@anu.edu.au

- [1] C. Weisbuch, M. Nishioka, A. Ishikawa, and Y. Arakawa, Observation of the coupled exciton-photon mode splitting in a semiconductor quantum microcavity, *Phys. Rev. Lett.* **69**, 3314 (1992).
- [2] J. Kasprzak, M. Richard, S. Kundermann, A. Baas, P. Jeambrun, J. M. Keeling, F. M. Marchetti, M. H. Szymńska, R. André, J. L. Staehli, V. Savona, P. B. Littlewood, B. Deveaud, and L. S. Dang, Bose-Einstein condensation of exciton polaritons, *Nature* **443**, 409 (2006).
- [3] A. Amo, J. Lefrère, S. Pigeon, C. Adrados, C. Ciuti, I. Carusotto, R. Houdré, E. Giacobino, and A. Bramati, Superfluidity of polaritons in semiconductor microcavities, *Nature Physics* **5**, 805 (2009).
- [4] T. Gao, E. Estrecho, K. Y. Bliokh, T. C. Liew, M. D. Fraser, S. Brodbeck, M. Kamp, C. Schneider, S. Höfling, Y. Yamamoto, F. Nori, Y. S. Kivshar, A. G. Truscott, R. G. Dall, and E. A. Ostrovskaya, Observation of non-Hermitian degeneracies in a chaotic exciton-polariton billiard, *Nature* **526**, 554 (2015).
- [5] C. Schneider, A. Rahimi-Iman, N. Y. Kim, J. Fischer, I. G. Savenko, M. Amthor, M. Lerner, A. Wolf, L. Worschech, V. D. Kulakovskii, I. A. Shelykh, M. Kamp, S. Reitzenstein, A. Forchel, Y. Yamamoto, and S. Höfling, An electrically pumped polariton laser, *Nature* **497**, 348 (2013).
- [6] S. Klembt, T. H. Harder, O. A. Egorov, K. Winkler, R. Ge, M. A. Bandres, M. Emmerling, L. Worschech, T. C. Liew, M. Segev, C. Schneider, and S. Höfling, Exciton-polariton topological insulator, *Nature* **562**, 552 (2018).
- [7] S. Christopoulos, G. B. H. von Högersthal, A. J. D. Grundy, P. G. Lagoudakis, A. V. Kavokin, J. J. Baumberg, G. Christmann, R. Butté, E. Feltin, J.-F. Carlin, and N. Grandjean, Room-temperature polariton lasing in semiconductor microcavities, *Phys. Rev. Lett.* **98**, 126405 (2007).
- [8] T. Guillet, M. Mexis, J. Levrat, G. Rossbach, C. Brimont, T. Bretagnon, B. Gil, R. Butté, N. Grandjean, L. Orosz, F. Réveret, J. Leymarie, J. Zúñiga-Pérez, M. Leroux, F. Semond, and S. Bouchoule, Polariton lasing in a hybrid bulk ZnO microcavity, *Applied Physics Letters* **99**, 161104 (2011).
- [9] R. Su, C. Diederichs, J. Wang, T. C. H. Liew, J. Zhao, S. Liu, W. Xu, Z. Chen, and Q. Xiong, Room-temperature polariton lasing in all-inorganic perovskite nanoplatelets, *Nano Letters* **17**, 3982 (2017).
- [10] C. P. Dietrich, A. Steude, L. Tropic, M. Schubert, N. M. Kronenberg, K. Ostermann, S. Höfling, and M. C. Gather, An exciton-polariton laser based on biologically produced fluorescent protein, *Science Advances* **2**, 8 (2016).
- [11] M. Dusel, S. Betzold, T. H. Harder, M. Emmerling, J. Beierlein, J. Ohmer, U. Fischer, R. Thomale, C. Schneider, S. Höfling, and S. Klembt, Room-temperature topological polariton laser in an organic lattice, *Nano Letters* **21**, 6398 (2021).
- [12] G. Lerario, A. Fieramosca, F. Barachati, D. Ballarini, K. S. Daskalakis, L. Dominici, M. D. Giorgi, S. A. Maier, G. Gigli, S. Kéna-Cohen, and D. Sanvitto, Room-temperature superfluidity in a polariton condensate, *Nature Physics* **13**, 837 (2017).
- [13] R. Su, E. Estrecho, D. Biegańska, Y. Huang, M. Wurdack, M. Pieczarka, A. G. Truscott, T. C. H. Liew, E. A. Ostrovskaya, and Q. Xiong, Direct measurement of a non-hermitian topological invariant in a hybrid light-matter system, *Science Advances* **7**, 45 (2021).
- [14] R. Su, S. Ghosh, J. Wang, S. Liu, C. Diederichs, T. C. Liew, and Q. Xiong, Observation of exciton polariton condensation in a perovskite lattice at room temperature, *Nature Physics* **16**, 301 (2020).
- [15] K. F. Mak, C. Lee, J. Hone, J. Shan, and T. F. Heinz, Atomically thin MoS_2 : A new direct-gap semiconductor, *Phys. Rev. Lett.* **105**, 136805 (2010).
- [16] X. Liu, T. Galfsky, Z. Sun, F. Xia, E. C. Lin, Y. H. Lee, S. Kéna-Cohen, and V. M. Menon, Strong light-matter coupling in two-dimensional atomic crystals, *Nature Photonics* **9**, 30 (2014).
- [17] D. Sanvitto and S. Kéna-Cohen, The road towards polaritonic devices, *Nature Materials* **15**, 1061 (2016).

- [18] C. Schneider, M. M. Glazov, T. Korn, S. Höfling, and B. Urbaszek, Two-dimensional semiconductors in the regime of strong light-matter coupling, *Nature Communications* **9**, 2695 (2018).
- [19] J. Gu, B. Chakraborty, M. Khatoniar, and V. M. Menon, A room-temperature polariton light-emitting diode based on monolayer WS₂, *Nature Nanotechnology* **14**, 1024 (2019).
- [20] T. Yun, M. Wurdack, M. Pieczarka, S. Bhattacharyya, Q. Ou, C. Notthoff, C. K. Nguyen, T. Daeneke, P. Kluth, M. S. Fuhrer, A. G. Truscott, E. Estrecho, and E. A. Ostrovskaya, Influence of direct deposition of dielectric materials on the optical response of monolayer WS₂, *Applied Physics Letters* **119**, 133106 (2021).
- [21] N. Lundt, S. Klemmt, E. Cherotchenko, S. Betzold, O. Iff, A. V. Nalitov, M. Klaas, C. P. Dietrich, A. V. Kavokin, S. Höfling, and C. Schneider, Room-temperature Tamm-plasmon exciton-polaritons with a WSe₂ monolayer, *Nature Communications* **7**, 2695 (2016).
- [22] Y. J. Chen, J. D. Cain, T. K. Stanev, V. P. Dravid, and N. P. Stern, Valley-polarized exciton-polaritons in a monolayer semiconductor, *Nature Photonics* **11**, 431 (2017).
- [23] N. Lundt, Lukasz Dusanowski, E. Sedov, P. Stepanov, M. M. Glazov, S. Klemmt, M. Klaas, J. Beierlein, Y. Qin, S. Tongay, M. Richard, A. V. Kavokin, S. Höfling, and C. Schneider, Optical valley Hall effect for highly valley-coherent exciton-polaritons in an atomically thin semiconductor, *Nature Nanotechnology* **14**, 770 (2019).
- [24] C. Rupprecht, N. Lundt, M. Wurdack, P. Stepanov, E. Estrecho, M. Richard, E. A. Ostrovskaya, S. Höfling, and C. Schneider, Micro-mechanical assembly and characterization of high-quality Fabry-Pérot microcavities for the integration of two-dimensional materials, *Applied Physics Letters* **118**, 103103 (2021).
- [25] M. Wurdack, E. Estrecho, S. Todd, T. Yun, M. Pieczarka, S. K. Earl, J. A. Davis, C. Schneider, A. G. Truscott, and E. A. Ostrovskaya, Motional narrowing, ballistic transport, and trapping of room-temperature exciton polaritons in an atomically-thin semiconductor, *Nature Communications* **12**, 5366 (2021).
- [26] C. Anton-Solanas, M. Waldherr, M. Klaas, H. Suchomel, T. H. Harder, H. Cai, E. Sedov, S. Klemmt, A. V. Kavokin, S. Tongay, K. Watanabe, T. Taniguchi, S. Höfling, and C. Schneider, Bosonic condensation of exciton-polaritons in an atomically thin crystal, *Nature Materials* **20**, 1233 (2021).
- [27] J. Zhao, A. Fieramosca, R. Bao, W. Du, K. Dini, R. Su, J. Feng, Y. Luo, D. Sanvitto, T. C. Liew, and Q. Xiong, Nonlinear polariton parametric emission in an atomically thin semiconductor based microcavity, *Nature Nanotechnology* **17**, 396 (2022).
- [28] H. Knopf, N. Lundt, T. Bucher, S. Höfling, S. Tongay, T. Taniguchi, K. Watanabe, I. Staudé, U. Schulz, C. Schneider, and F. Eilenberger, Integration of atomically thin layers of transition metal dichalcogenides into high-Q, monolithic Bragg-cavities: an experimental platform for the enhancement of the optical interaction in 2D-materials, *Optical Materials Express* **9**, 598 (2019).
- [29] H. Shan, L. Lackner, B. Han, E. Sedov, C. Rupprecht, H. Knopf, F. Eilenberger, J. Beierlein, N. Kunte, M. Esmann, K. Yumigeta, K. Watanabe, T. Taniguchi, S. Klemmt, S. Höfling, A. V. Kavokin, S. Tongay, C. Schneider, and C. Antón-Solanas, Spatial coherence of room-temperature monolayer WSe₂ exciton-polaritons in a trap, *Nature Communications* **12**, 6406 (2021).
- [30] M. Waldherr, N. Lundt, M. Klaas, S. Betzold, M. Wurdack, V. Baumann, E. Estrecho, A. Nalitov, E. Cherotchenko, H. Cai, E. A. Ostrovskaya, A. V. Kavokin, S. Tongay, S. Klemmt, S. Höfling, and C. Schneider, Observation of bosonic condensation in a hybrid monolayer MoSe₂-GaAs microcavity, *Nature Communications* **9**, 3286 (2018).
- [31] N. Lundt, P. Nagler, A. Nalitov, S. Klemmt, M. Wurdack, S. Stoll, T. H. Harder, S. Betzold, V. Baumann, A. V. Kavokin, C. Schüller, T. Korn, S. Höfling, and C. Schneider, Valley polarized relaxation and upconversion luminescence from Tamm-plasmon trion-polaritons with a MoSe₂ monolayer, *2D Materials* **4**, 025096 (2017).
- [32] M. Wurdack, N. Lundt, M. Klaas, V. Baumann, A. V. Kavokin, S. Höfling, and C. Schneider, Observation of hybrid Tamm-plasmon exciton-polaritons with GaAs quantum wells and a MoSe₂ monolayer, *Nature Communications* **8**, 259 (2017).
- [33] J. Gu, V. Walther, L. Waldecker, D. Rhodes, A. Raja, J. C. Hone, T. F. Heinz, S. Kéna-Cohen, T. Pohl, and V. M. Menon, Enhanced nonlinear interaction of polaritons via excitonic rydberg states in monolayer WSe₂, *Nature Communications* **12**, 2269 (2021).
- [34] B. Datta, M. Khatoniar, P. Deshmukh, R. Bushati, S. De Liberato, S. K. Cohen, and V. M. Menon, Highly non-linear interlayer exciton-polaritons in bilayer MoS₂, arXiv:2110.13326 (2021).
- [35] J. Zhao, R. Su, A. Fieramosca, W. Zhao, W. Du, X. Liu, C. Diederichs, D. Sanvitto, T. C. H. Liew, and Q. Xiong, Ultralow threshold polariton condensate in a monolayer semiconductor microcavity at room temperature, *Nano Letters* **21**, 3331 (2021).
- [36] The fabrication of the high-reflectivity substrate was performed at the ACT OptoFab node of the Australian National Fabrication Facility - a company established under the National Collaborative Research Infrastructure Strategy to provide nano and microfabrication facilities for Australia's researchers.
- [37] A. Kavokin, J. Baumberg, G. Malpuech, and F. Laussy, *Microcavities*, Series on Semiconductor Science and Technology (OUP Oxford, 2017).
- [38] <http://www.hqgraphene.com>.
- [39] <http://www.novawafers.com>.
- [40] H. Zeng, G. B. Liu, J. Dai, Y. Yan, B. Zhu, R. He, L. Xie, S. Xu, X. Chen, W. Yao, and X. Cui, Optical signature of symmetry variations and spin-valley coupling in atomically thin tungsten dichalcogenides, *Scientific Reports* **3**, 1608 (2013).
- [41] T. Mueller and E. Malic, Exciton physics and device application of two-dimensional transition metal dichalcogenide semiconductors, *npj 2D Materials and Applications* **2**, 29 (2018).
- [42] N. Lundt, A. Maryński, E. Cherotchenko, A. Pant, X. Fan, S. Tongay, G. Sek, A. V. Kavokin, S. Höfling, and C. Schneider, Monolayered MoSe₂: a candidate for room temperature polaritonics, *2D Materials* **4**, 015006 (2016).
- [43] S. Tongay, J. Suh, C. Ataca, W. Fan, A. Luce, J. S. Kang, J. Liu, C. Ko, R. Raghunathanan, J. Zhou, F. Ogletree, J. Li, J. C. Grossman, and J. Wu, Defects activated photoluminescence in two-dimensional semiconductors: Interplay between bound, charged, and free excitons, *Sci-*

- entific Reports **3**, 2657 (2013).
- [44] J. Shang, X. Shen, C. Cong, N. Peimyoo, B. Cao, M. Eginligil, and T. Yu, Observation of excitonic fine structure in a 2D transition-metal dichalcogenide semiconductor, *ACS Nano* **9**, 647 (2015).
- [45] V. Carozo, Y. Wang, K. Fujisawa, B. R. Carvalho, A. McCreary, S. Feng, Z. Lin, C. Zhou, N. Perea-López, A. L. Elías, B. Kabiús, V. H. Crespi, and M. Terrones, Optical identification of sulfur vacancies: Bound excitons at the edges of monolayer tungsten disulfide, *Science Advances* **3**, 4 (2017).
- [46] R. Sebait, C. Biswas, B. Song, C. Seo, and Y. H. Lee, Identifying defect-induced trion in monolayer WS₂ via carrier screening engineering, *ACS Nano* **15**, 2849 (2021).
- [47] S. Tongay, J. Zhou, C. Ataca, J. Liu, J. S. Kang, T. S. Matthews, L. You, J. Li, J. C. Grossman, and J. Wu, Broad-range modulation of light emission in two-dimensional semiconductors by molecular physisorption gating, *Nano Letters* **13**, 2831 (2013).
- [48] F. Zhang, Y. Lu, D. S. Schulman, T. Zhang, K. Fujisawa, Z. Lin, Y. Lei, A. L. Elías, S. Das, S. B. Sinnott, and M. Terrones, Carbon doping of WS₂ monolayers: Bandgap reduction and p-type doping transport, *Science Advances* **5**, 5 (2019).
- [49] J. Gao, B. Li, J. Tan, P. Chow, T.-M. Lu, and N. Koratkar, Aging of transition metal dichalcogenide monolayers, *ACS Nano* **10**, 2628 (2016).
- [50] B. Charlot, S. Gauthier, A. Garraud, P. Combette, and A. Giani, PvdF/pmma blend pyroelectric thin films, *Journal of Materials Science: Materials in Electronics* **22**, 1766 (2011).
- [51] K. F. Mak, K. He, C. Lee, G. H. Lee, J. Hone, T. F. Heinz, and J. Shan, Tightly bound trions in monolayer MoS₂, *Nature Materials* **12**, 207 (2013).
- [52] B. Zhu, X. Chen, and X. Cui, Exciton binding energy of monolayer WS₂, *Scientific Reports* **5**, 9218 (2015).
- [53] J. Martín-Sánchez, A. Mariscal, M. D. Luca, A. T. Martín-Luengo, G. Gramse, A. Halilovic, R. Serna, A. Bonanni, I. Zardo, R. Trotta, and A. Rastelli, Effects of dielectric stoichiometry on the photoluminescence properties of encapsulated WSe₂ monolayers, *Nano Research* **11**, 1399 (2018).
- [54] M. Born, E. Wolf, and A. Bhatia, *Principles of Optics: Electromagnetic Theory of Propagation, Interference and Diffraction of Light* (Cambridge University Press, 2000).
- [55] Y. Li, A. Chernikov, X. Zhang, A. Rigosi, H. M. Hill, A. M. van der Zande, D. A. Chenet, E.-M. Shih, J. Hone, and T. F. Heinz, Measurement of the optical dielectric function of monolayer transition-metal dichalcogenides: MoS₂, MoSe₂, WS₂, and WSe₂, *Phys. Rev. B* **90**, 205422 (2014).
- [56] Z. Khatibi, M. Feierabend, M. Selig, S. Brem, C. Linderälv, P. Erhart, and E. Malic, Impact of strain on the excitonic linewidth in transition metal dichalcogenides, *2D Materials* **6**, 015015 (2018).
- [57] K. He, C. Poole, K. F. Mak, and J. Shan, Experimental demonstration of continuous electronic structure tuning via strain in atomically thin MoS₂, *Nano Letters* **13**, 2931 (2013).
- [58] M. Sidler, P. Back, O. Cotlet, A. Srivastava, T. Fink, M. Kroner, E. Demler, and A. Imamoglu, Fermi polaron-polaritons in charge-tunable atomically thin semiconductors, *Nature Physics* **13**, 255 (2017).
- [59] V. Savona, L. Andreani, P. Schwendimann, and A. Quattropani, Quantum well excitons in semiconductor microcavities: Unified treatment of weak and strong coupling regimes, *Solid State Communications* **93**, 733 (1995).
- [60] J. Lee, S. Pak, P. Giraud, Y.-W. Lee, Y. Cho, J. Hong, A.-R. Jang, H.-S. Chung, W.-K. Hong, H. Y. Jeong, H. S. Shin, L. G. Occhipinti, S. M. Morris, S. Cha, J. I. Sohn, and J. M. Kim, Thermodynamically stable synthesis of large-scale and highly crystalline transition metal dichalcogenide monolayers and their unipolar n-n heterojunction devices, *Advanced Materials* **29**, 1702206 (2017).
- [61] S. H. Choi, S. J. Yun, Y. S. Won, C. S. Oh, S. M. Kim, K. K. Kim, and Y. H. Lee, Large-scale synthesis of graphene and other 2D materials towards industrialization, *Nature Communications* **13**, 1484 (2022).
- [62] S. B. Desai, S. R. Madhvapathy, M. Amani, D. Kiriya, M. Hettick, M. Tosun, Y. Zhou, M. Dubey, J. W. Ager III, D. Chrzan, and A. Javey, Gold-mediated exfoliation of ultralarge optoelectronically-perfect monolayers, *Advanced Materials* **28**, 4053 (2016).
- [63] F. Liu, W. Wu, Y. Bai, S. H. Chae, Q. Li, J. Wang, J. Hone, and X.-Y. Zhu, Disassembling 2d van der waals crystals into macroscopic monolayers and reassembling into artificial lattices, *Science* **367**, 903 (2020).
- [64] R. Su, J. Wang, J. Zhao, J. Xing, W. Zhao, C. Diederichs, T. C. H. Liew, and Q. Xiong, Room temperature long-range coherent exciton polariton condensate flow in lead halide perovskites, *Science Advances* **4**, 10 (2018).

Supplementary Material:
Fabrication of high-quality PMMA/SiO_x spaced planar microcavities for strong coupling of light with monolayer WS₂ excitons

Tinghe Yun,^{1,2,3} Eliezer Estrecho,¹ Andrew G. Truscott,⁴ Elena A. Ostrovskaya,^{1,*} and Matthias J. Wurdack^{1,†}

¹*ARC Centre of Excellence in Future Low-Energy Electronics Technologies and Department of Quantum Science and Technology, Research School of Physics, The Australian National University, Canberra, ACT 2601, Australia*

²*Songshan Lake Materials Laboratory, Dongguan 523808, Guangdong, China*

³*Institute of Physics, Chinese Academy of Science, Beijing, 100190, China*

⁴*Department of Quantum Science and Technology, Research School of Physics, The Australian National University, Canberra, ACT 2601, Australia*

(Dated: September 29, 2022)

S1: SUMMARY OF FABRICATION PROCEDURES AND Q-FACTORS OF TMDC-BASED MICROCAVITIES

| Cavity Architecture | Spacer Material | Fabrication Technique | Q-factor | Ref |
|---|--|--|----------|----------|
| Open microcavity with a concave cavity spacer | Air gap | DBR deposition on separate substrates. | ~ 4200 | [1] |
| Open microcavity | Air gap | DBR deposition on separate substrates. | ~ 160 | [2] |
| All-dielectric microcavity | SiO ₂ | Bottom-up deposition by PECVD. | ~ 250 | [3, 4] |
| DBR/metal cavity | SiO ₂ /h-BN/PMMA | Bottom-up deposition of DBR by PECVD, hexagonal Boron Nitride (hBN) by mechanical transfer, PMMA spacer by spin-coating and top metal mirror by electron beam evaporation (EBE). | ~ 78 | [5] |
| DBR/metal cavity | SiO ₂ /PMMA | Bottom-up deposition of DBR by sputtering, PMMA spacer by spin-coating and top metal mirror by EBE. | ~ 110 | [6] |
| DBR/metal cavity | AlAs/GaInP/PMMA | Bottom-up deposition of DBR and cavity spacer by molecular beam epitaxy (MBE), PMMA spacer by spin-coating and top metal layer by EBE. | ~ 650 | [7] |
| All-dielectric microcavity | SiO ₂ /HSQ/Al ₂ O ₃ | Bottom-up deposition of DBR substrate by PECVD, hydrogen silsesquioxane (HSQ) spacer by spin-coating, Al ₂ O ₃ spacer by atomic-layer deposition (ALD) and top DBR by PECVD. | ~ 600 | [8, 9] |
| All-dielectric microcavity | hBN/SiO ₂ | Bottom-up deposition of DBR substrate by ion-assisted physical vapor deposition (IAD), hBN via mechanical transfer, and SiO ₂ spacer and top DBR via IAD. | ~ 4500 | [10, 11] |
| “Flip-Chip” microcavity | PMMA/SiO ₂ | Deposition of DBR substrate by sputtering, PMMA spacer by spin-coating and mechanical transfer of the top DBR. | ~ 4500 | [12, 13] |
| “Flip-Chip” all-dielectric microcavity | SiO ₂ | Deposition of DBR substrate by PECVD and sputtering, and mechanical transfer of the top DBR. | ~ 3000 | [13, 14] |
| This work | PMMA/SiO _x | Bottom-up deposition of DBR substrate by sputtering, PMMA spacer by spin-coating, and SiO _x spacer and top DBR by PECVD. | ~ 3500 | |

TABLE S1. Summary of fabrication procedures and Q-factors of planar microcavities with integrated monolayer TMDCs operating in the strong exciton-photon coupling regime.

S2: DEPOSITION OF THE SILICON OXIDE SPACER AND THE TOP DBR

The SiO_x spacer on top of the PMMA, and the top $\text{SiN}_x/\text{SiO}_x$ DBR were deposited via plasma enhanced chemical vapour deposition (PECVD) using the Oxford PlasmaLab System 100 operating at radio frequency (RF). The pressure of the PECVD chamber was set to $p = 650$ mTor, the temperature to $T = 150$ °C and the power of the RF generator to $P = 30$ W. For the SiO_x deposition, we introduced 161 sccm of N_2 gas, 710 sccm of N_2O gas and 9 sccm of SiH_4 gas, and for the SiN_x deposition, 980 sccm of N_2 gas, 14 sccm of NH_3 gas and 18 sccm of SiH_4 gas into the deposition chamber. The growth rates and the refractive indices of the deposited SiN_x and SiO_x layers were initially determined via ellipsometry, ensuring that the layers meet the Bragg condition for light with the wavelength of the WS_2 excitons, $\lambda_C \approx \lambda_X$.

S3: CROSS SECTION OF THE ANGLE-RESOLVED PL SPECTRUM

To extract the peak energies of the angle-resolved PL spectrum of the loaded microcavity (shown in the manuscript Fig. 5d), we fitted to each spectrum shown in Fig. S1 a two-peak Voigt function, which are plotted together with the cavity mode on the position of the monolayer as reference. The fitted peak positions are marked in Fig. 5d and follow well the expected lower and upper polariton branches in this system.

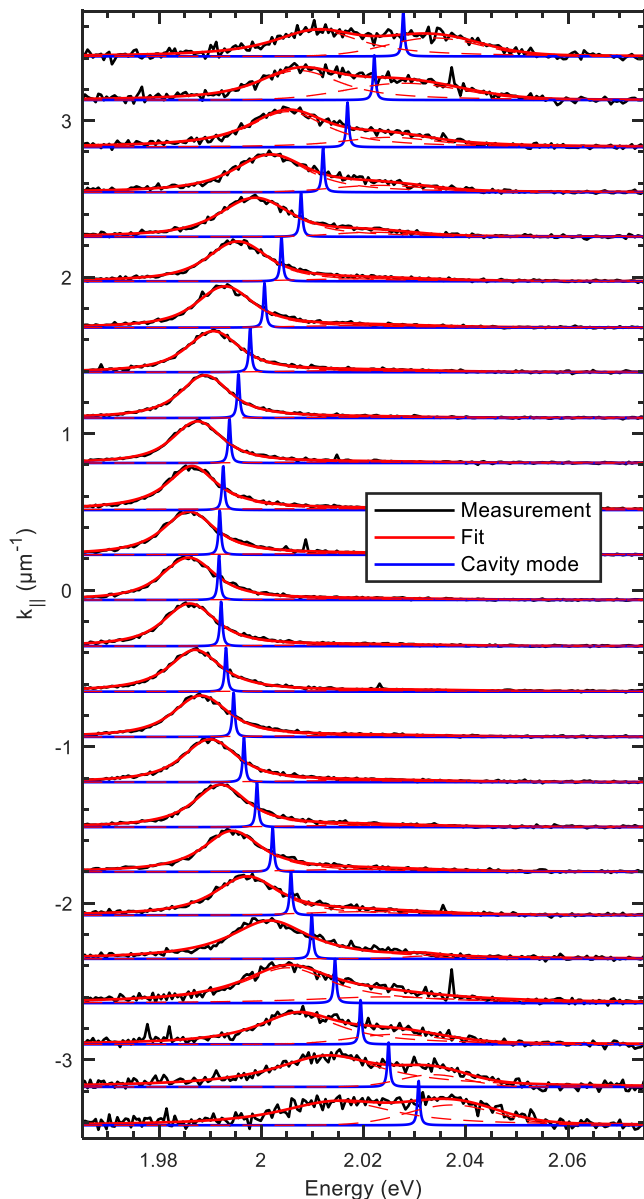


FIG. S1. Normalised PL spectra extracted from the angle-resolved PL measurement of the loaded microcavity (see manuscript Fig. 5d), fitted with two-peak Voigt functions, where the baseline of each spectrum marks its corresponding in-plane momentum. The cavity mode at the position of the WS_2 monolayer is plotted as a reference.

* elena.ostrovskaya@anu.edu.au

† matthias.wurdack@anu.edu.au

- [1] M. Sidler, P. Back, O. Cotlet, A. Srivastava, T. Fink, M. Kroner, E. Demler, and A. Imamoglu, Fermi polaron-polaritons in charge-tunable atomically thin semiconductors, *Nature Physics* **13**, 255 (2017).
- [2] M. Król, K. Lekenta, R. Mirek, K. Lempicka, D. Stephan, K. Nogajewski, M. R. Molas, A. Babiński, M. Potemski, J. Szczytko, and B. Pietka, Valley polarization of exciton-polaritons in monolayer WSe_2 in a tunable microcavity, *Nanoscale* **11**, 9574 (2019).
- [3] X. Liu, T. Galfsky, Z. Sun, F. Xia, E. C. Lin, Y. H. Lee, S. Kéna-Cohen, and V. M. Menon, Strong light-matter coupling in two-dimensional atomic crystals, *Nature Photonics* **9**, 30 (2014).
- [4] Y. J. Chen, J. D. Cain, T. K. Stanev, V. P. Dravid, and N. P. Stern, Valley-polarized exciton-polaritons in a monolayer semiconductor, *Nature Photonics* **11**, 431 (2017).
- [5] J. Gu, B. Chakraborty, M. Khatoniari, and V. M. Menon, A room-temperature polariton light-emitting diode based

on monolayer WS_2 , *Nature Nanotechnology* **14**, 1024 (2019).

- [6] N. Lundt, S. Klemmt, E. Cherotchenko, S. Betzold, O. Iff, A. V. Nalitov, M. Klaas, C. P. Dietrich, A. V. Kavokin, S. Höfling, and C. Schneider, Room-temperature Tamm-plasmon exciton-polaritons with a WSe_2 monolayer, *Nature Communications* **7**, 2695 (2016).
- [7] M. Wurdack, N. Lundt, M. Klaas, V. Baumann, A. V. Kavokin, S. Höfling, and C. Schneider, Observation of hybrid Tamm-plasmon exciton-polaritons with GaAs quantum wells and a MoSe_2 monolayer, *Nature Communica-*

- tions **8**, 259 (2017).
- [8] X. Liu, W. Bao, Q. Li, C. Ropp, Y. Wang, and X. Zhang, Control of coherently coupled exciton polaritons in monolayer tungsten disulphide, *Phys. Rev. Lett.* **119**, 027403 (2017).
- [9] X. Liu, J. Yi, Q. Li, S. Yang, W. Bao, C. Ropp, S. Lan, Y. Wang, and X. Zhang, Nonlinear optics at excited states of exciton polaritons in two-dimensional atomic crystals, *Nano Letters* **20**, 1676 (2020).
- [10] H. Knopf, N. Lundt, T. Bucher, S. Höfling, S. Tongay, T. Taniguchi, K. Watanabe, I. Staude, U. Schulz, C. Schneider, and F. Eilenberger, Integration of atomically thin layers of transition metal dichalcogenides into high-Q, monolithic Bragg-cavities: an experimental platform for the enhancement of the optical interaction in 2D-materials, *Optical Materials Express* **9**, 598 (2019).
- [11] H. Shan, L. Lackner, B. Han, E. Sedov, C. Rupperecht, H. Knopf, F. Eilenberger, J. Beierlein, N. Kunte, M. Esmann, K. Yumigeta, K. Watanabe, T. Taniguchi, S. Klemmt, S. Höfling, A. V. Kavokin, S. Tongay, C. Schneider, and C. Antón-Solanas, Spatial coherence of room-temperature monolayer WSe₂ exciton-polaritons in a trap, *Nature Communications* **12**, 6406 (2021).
- [12] N. Lundt, Łukasz Dusanowski, E. Sedov, P. Stepanov, M. M. Glazov, S. Klemmt, M. Klaas, J. Beierlein, Y. Qin, S. Tongay, M. Richard, A. V. Kavokin, S. Höfling, and C. Schneider, Optical valley Hall effect for highly valley-coherent exciton-polaritons in an atomically thin semiconductor, *Nature Nanotechnology* **14**, 770 (2019).
- [13] C. Rupperecht, N. Lundt, M. Wurdack, P. Stepanov, E. Estrecho, M. Richard, E. A. Ostrovskaya, S. Höfling, and C. Schneider, Micro-mechanical assembly and characterization of high-quality Fabry-Pérot microcavities for the integration of two-dimensional materials, *Applied Physics Letters* **118**, 103103 (2021).
- [14] M. Wurdack, E. Estrecho, S. Todd, T. Yun, M. Pieczarka, S. K. Earl, J. A. Davis, C. Schneider, A. G. Truscott, and E. A. Ostrovskaya, Motional narrowing, ballistic transport, and trapping of room-temperature exciton polaritons in an atomically-thin semiconductor, *Nature Communications* **12**, 5366 (2021).